NASA CONTRACTOR
REPORT

NASA CR-129034

INVESTIGATION OF SOLIDIFICATION IN ZERO-GRAVITY ENVIRONMENT: M553 SPHERE FORMING EXPERIMENT

Nickel - Silver Alloy Evaluation

By Theo Z. Kattamis
University of Connecticut
Waterbury, Connecticut 06710

December 1973

Prepared for

NASA-GEORGE C. MARSHALL SPACE FLIGHT CENTER
Marshall Space Flight Center, Alabama 35812

TECHNICAL REPORT STANDARD TITLE PAGE

1. REPORT NO.	2. GOVERNMENT ACCESSION NO.	3. RECIPIENT'S CATALOG NO.
NASA CR-129034		

4. TITLE AND SUBTITLE	5. REPORT DATE
Investigation of Solidification in Zero-Gravity Environment; M553 Sphere Forming Experiment Nickel - Silver Alloy Evaluation	December 1973
	6. PERFORMING ORGANIZATION CODE
7. AUTHOR(S) Theo Z. Kattamis	8. PERFORMING ORGANIZATION REPORT #
9. PERFORMING ORGANIZATION NAME AND ADDRESS University of Connecticut Waterbury, Connecticut 06710	10. WORK UNIT NO.
	11. CONTRACT OR GRANT NO. NAS 8-28734
12. SPONSORING AGENCY NAME AND ADDRESS National Aeronautics and Space Administration Washington, D. C. 20546	13. TYPE OF REPORT & PERIOD COVERED May 1972 - December 1973 Contractor Report
	14. SPONSORING AGENCY CODE

15. SUPPLEMENTARY NOTES

16. ABSTRACT

Five Nickel-1 wt% silver specimens were processed in space. Four among them (SL-1.2, SL-1.12, SL-1.13 and SL-2.8) melted only partially, whereas the fifth (SL-2.4) melted completely and assumed after solidification a perfectly spherical shape. Growth of the solid was epitaxial on the unmelted material or on the retaining sting (SL-2.4) and occurred without undercooling. Solidification was dendritic in all cases with nonequilibrium silver particles forming monotectically between dendrite arms. Substantial loss of silver by evaporation took place. Evaporation of silver within internal gas cavities in the melt was followed by surface condensation after completion of solidification and cooling, leading to a silver-rich lining of these cavities. This material gave no microstructural evidence of any reduction in liquid convection.

17. KEY WORDS	18. DISTRIBUTION STATEMENT
	Unclassified - Unlimited Th. Kattamis

19. SECURITY CLASSIF. (of this report)	20. SECURITY CLASSIF. (of this page)	21. NO. OF PAGES	22. PRICE
Unclassified	Unclassified	20	NTIS

TABLE OF CONTENTS

	Page
Summary	1
Characterization Results	1
Sphericity	1
Density, Porosity	1
Surface Topography	2
Grain Formation	2
Dendritic Structure	3
Segregation	3
Nonmetallic Inclusions	4
Microhardness Survey	4
Chemical Composition	5
Discussion	5
Conclusions	6
References	7

LIST OF ILLUSTRATIONS

Figure	Title	Page
1.	Shadowgraphs (10X) and X-ray macroradiographs (1X) of specimen SL-2.4. (a) Top views, (b)and (c) side views	8
2.	Scanning electron micrographs of specimen SL-1.13. (a) 10X, (b) 50X and (c) 150X. Courtesy of Grumman Aerospace Corporation	9
3.	Scanning electron micrographs of specimen SL-1.2. (a) 10X, (b) dendritic morphology within a cavity, 250X, (c) cellular solidification pattern within the web of the specimen, 750X, and (d) inner surface patterns in upper cavity, 1500X. Courtesy of Grumman Aerospace Corporation	10
4.	Scanning electron micrographs of specimen SL-2.8. (a) 10X, (b) 25X and (c) 100X	11
5.	Scanning electron micrographs of specimen SL-2.4. (a) 10X, (b) 25X, (c) and (d) 100X	12
6.	Photomicrographs illustrating the microstructure of specimen SL-1.12 (Courtesy of A. D. Little, Inc.) and of specimens SL-2.4 and SL-2.8, 10X	13
7.	Photomicrographs of specimen SL-1.12. (a) 50X, (b) 125X. Courtesy of A. D. Little, Inc.	14
8.	(a) Photomicrograph of specimen SL-1.13, 200X. (b) Scanning electron micrograph of specimen SL-1.13, 1500X	15
9.	Photomicrographs of specimen SL-2.8. (a) Polarized light, 100X, (b) 50X, (c) and (d) 100X	16
10.	Photomicrographs of specimen SL-2.4 etched with Rosenhain's reagent. (a) 25X, (b) and (c) 50X and (d) 100X.	17

NICKEL-SILVER ALLOY EVALUATION

Summary

Five nickel-1 wt% silver specimens were processed in space. Four among them (SL-1.2, SL-1.12, SL-1.13 and SL-2.8) melted only partially, whereas the fifth (SL-2.4) melted completely and assumed after solidification a perfectly spherical shape. Growth of the solid was epitaxial on the unmelted material or on the retaining sting (SL-2.4) and occurred without undercooling. Solidification was dendritic in all cases with nonequilibrium silver particles forming monotectically between dendrite arms. Substantial loss of silver by evaporation took place. Evaporation of silver within internal gas cavities in the melt was followed by surface condensation after completion of solidification and cooling, leading to a silver-rich lining of these cavities. This material gave no microstructural evidence of any reduction in liquid convection.

Characterization Results

Five nickel-silver specimens were processed in space. They were studied as follows: Grumman Aerospace, specimens SL-1.2 and SL-1.13; Arthur D. Little, Inc., specimen SL-1.12; and University of Connecticut, specimens SL-2.4 and SL-2.8.

Sphericity. Specimens SL-1.2, SL-1.12, SL-1.13 and SL-2.8 are grossly misshaped, mainly because of incomplete melting. Specimen SL-2.4 is perfectly spherical with a radius equal to 0.275 ± 0.005 cms as established by micrometric and shadowgraphic examinations, Figure 1.

Density, Porosity. The density of the five specimens varied between 6.12 gm/cm^3 for specimen SL-1.12 and 8.90 gm/cm^3 for specimen SL-2.4. This variation was caused by internal microporosity and especially macroporosity. Thus, in specimen SL-1.12 a large macropore (3.4 mm in diameter) was detected, together with five smaller others (one 1.7 mm in diameter, two about 0.6 mm, another about 0.3 mm and a small one 0.1 mm in diameter). The volume

percent microporosity was calculated from density considerations and by quantitative metallography. Very fine microporosity was evaluated by quantitative measurements made on X-ray microradiographs. Specimen SL-2.4 exhibited the lowest volume percent microporosity, equal to 1.01.

Surface Topography. The surface of all specimens with the exception of specimen SL-2.4, is rough with peculiar patterns that may be attributed to flow of mushy liquid, selective evaporation and thermal grooving, and to surface solidification shrinkage. Figure 2 illustrates the geometry and surface topography of specimen SL-1.13. A very large cavity is contained under the dome (A). The surface terracing of Figure 2b is difficult to interpret genetically, whereas the pattern of Figure 2c may be due to viscous flow of mushy liquid or to selective evaporation of silver, revealing the high nickel cores of surface dendrites. Figure 3 (1) illustrates the surface morphology of specimen SL-1.2. More specifically, Figure 3b illustrates a dendritic structure lining a large cavity, whereas Figure 3c illustrates a cellular structure with pronounced growth terraces. No silver precipitation has been detected at dendrite arm or cell boundaries. Quite peculiar is the surface topography within cells that is observed on the walls of a cavity, Figure 3d. The observed striations are most probably growth terraces. According to Larson (1) they might be plastic deformation markings generated during the sudden growth of the cavity (bubble), detected by telemetry. Figure 4 exhibits irregular patterns on the surface of specimen SL-2.8. Figure 5 illustrates the surface of specimen SL-2.4. This surface is extremely smooth with only a few grain boundaries that are grooved. No surface dendritic pattern is seen, presumably because the specimen lost a considerable amount of its silver by evaporation. This absence of surface dendrites, hence of interdendritic solidification shrinkage, is thought to be partly responsible for the surface smoothness.

Grain Formation. In specimens that were only partially melted, epitaxial growth on the unmelted solid (A) is observed. This growth may be columnar or equiaxed. In specimens that were in contact with the ceramic substrate, columnar growth is observed normal to the substrate surface. As examples of grain formation the columnar structure (B) in specimen SL-1.12 has an average width of 165 microns and an average length of 1135 microns. The equiaxed structure (C) has an average grain size of 210 microns. A second columnar structure (D) (width about 315 microns and length 1450 microns) grows

against the substrate. Under the surface cap and adjacent to the top of the pore is a mixed region of fine equiaxed grains of average size = 50 microns. In specimen SL-2.8 structure is columnar (B) with grains of average length = 900 microns and width = 210 microns, and equiaxed (C) with average grain size = 100 microns. Finally, in specimen SL-2.4 grain size is very coarse (1010 microns). The surface layer comprises only five grains. All grains are equiaxed dendritic and there is evidence that secondary grain growth has taken place.

Dendritic Structure. In specimen SL-1.12, Figure 7, the top cap above the large major pore includes a surface zone (E) that consists of very coarse dendrite cells of average size = 95 microns, and a zone (F) that consists of very fine equiaxed dendrites (average secondary dendrite arm spacing = 8 microns). Within the columnar structure (B), Figure 6, the spacing varies between 6 microns next to the unmelted specimen and 14 microns near the contact between equiaxed and columnar structures. Figure 8a illustrates the bulk microstructure of specimen SL-1.2. Grain boundaries and to a certain extent the grains are decorated by etch-pits that correspond to lattice defects and quite probably to precipitated silver particles. The intragranular pattern shown is reminiscent of a Frank-Read dislocation source. Figure 8b shows the nonequilibrium interdendritic silver precipitation that forms monotectically. The microstructure of specimen SL-2.8 is columnar dendritic (B) (secondary arm spacing = 25 microns next to the ceramic substrate and up to 40 microns at about 0.2 cm from the substrate), Figure 6, 9a and 9d, and equiaxed dendritic (C) (secondary arm spacing = 40 microns) close to the unmelted part of the specimen (A). The specimen SL-2.4 is coarse dendritic, consisting of "dendrite cells" of the primary nickel-rich phase, analogous to those observed in very slowly cooled alloys. Such "dendrite cells" of average size = 190 microns may be generated by extensive coarsening and coalescence that takes place during slow solidification. The interdendritic spaces appear to be richer in silver with locally recognizable silver particles, Figures 10b and d. Figure 10c indicates clearly that extensive grain growth has taken place after completion of solidification. Such a growth was made easier by the low amount of precipitated silver particles at "dendrite cell" boundaries.

Segregation. This two-phase monotectic alloy consists in the as-cast condition of primary dendrites of nickel-rich phase with

interdendritic discrete particles of a nonequilibrium phase that appears to be almost pure silver. These particles, whose volume percent depends on the actual amount of silver within the specimen, are very fine and are responsible for the formation of etch pits that appear as black spots delineating the secondary dendrite arm boundaries, Figure 9c. The appropriate way to define microsegregation in this system would have been by indicating the minimum silver concentration, C_m, measured along dendrite arm axes, and by the volume percent of nonequilibrium secondary phase (Ag). Accurate quantitative evaluation of this volume percent is practically impossible, because of its very low value. In specimen SL-2.8 the value of C_m = 0.55 wt% Ag was measured. Within the "dendrite cells" of specimen SL-2.4 no significant variation of silver concentration was measured. The average concentration was 0.49 wt% Ag. This specimen has lost an appreciable amount of silver by evaporation from the melt and to a lesser extent from the solid. A detailed investigation (1) of silver concentration within dendrites and along grain boundaries at locations close to the surface of specimen SL-1.2, in the bulk, and close to internal macropores indicated no meaningful differences. Silver concentrations at various points on the inner surface of the cavity in specimen SL-1.13 were measured by energy dispersive X-ray analysis in conjunction with scanning electron microscopy (1). Concentrations between 34 wt% Ag and 100 wt% Ag were reported (1). These high concentrations are encountered only on the surface of the cavity and may be attributed to condensation of silver vapor that filled the cavity. This condensation occurred during cooling of the specimen, following completion of solidification. The average silver concentration, measured in specimen SL-2.8, using a defocused electron beam, was 0.64 wt% in microstructure (B) and 0.72 wt% in microstructure (C). In specimen SL-2.4 it appeared to be uniform and equal to 0.52 wt%.

Nonmetallic Inclusions. Silica, silicoaluminates and sulfide particles of very fine sizes (about 1 micron) and in extremely small quantities were detected. Volume percent measurements appeared impossible to make.

Microhardness Survey. An average microhardness of 125 VHN was measured within the resolidified part of specimen SL-2.8, across both microstructures (B) and (C). A microhardness of 115 VHN was measured in specimen SL-2.4.

Chemical Composition. An investigation (1) of the surface chemistry of specimen SL-1.2 by energy dispersive X-ray analysis gave: (Ag: 0.77, Ni: 91.99, Cu: 0.90, Fe: 0.17, W: 0.05 and Al: 6.00). The high aluminum content is positively the result of contamination. X-ray fluorescence analysis (2) was conducted on the melted side of specimen SL-1.12 and indicated a tin content of about 0.5 wt% (probably from contamination) and a silver content of 1.36 wt%. In specimen SL-2.8 the silver concentration established by wet chemical analysis was 0.68 wt%. Other elements analyzed by procedures described elsewhere (3) were: (Mg: 5 ppm, Si: 5ppm, Cu: 15 ppm, Zn+ Pb: 15 ppm, O: 15 ppm, N: 5 ppm). In specimen SL-2.4 the silver concentration, determined by wet chemical analysis was 0.57 wt%. Other elements present were: (Mg: 3 ppm, Si: 3 ppm, Cu: 10 ppm, Zn + Pb: 10 ppm, O: 20 ppm and N: 20 ppm) (3).

Discussion

In the four specimens (SL-1.2, SL-1.2, SL-1.3 and SL-2.8) that melted partially, the unmelted part recrystallized due to the heat released by the adjacent solidifying metal. The melt solidified in a columnar dendritic fashion against the ceramic substrate and in some cases against the unmelted material. In other cases growth against the unmelted material was equiaxed. Because of the epitaxial character of growth the me'' did not undercool prior to nucleation of the solid. The specimen lost part of its silver by evaporation from the external surface of the melt or from internal surfaces of generated gas cavities. Silver vapor within these internal cavities condensed after solidification and subsequent cooling, lining their walls with a silver-rich layer. The minute silver particles that appear interdendritically and are minifested by etch-pits resulted from a monotectic reaction late during the solidification process. The solidification sequence of this alloy appears to be the following: nickel-rich dendrites grew from the melt while the temperature dropped from about the equilibrium liquidus to the monotectic temperature. At this temperature a silver-rich liquid separated, which with decreasing temperature became richer in silver by feeding with nickel-rich material the growing dendrites. The liquid composition finally reached pure silver and silver particles formed interdendritically. These specimens gave no evidence of any effect of zero-gravity environment on their microstructure or solidification behavior.

The specimen SL-2.4 melted completely and assumed a perfectly spherical shape. Solidification was dendritic with spacings of about 190 microns, that is about five times coarser than those observed in specimen SL-2.8 indicating very slow cooling. The reason for this very slow solidification is that this specimen was heated for about 25 seconds, hence superheated much more than the SL-2.8 specimen or the ground-processed specimens # 1-4 and # 1-11, which were heated for a shorter time (e.g. specimen SL-2.8 was heated for 15 seconds) and cooled down slower. Slow solidification is responsible for the extensive coarsening and coalescence that led to formation of coarse "dendrite cells" (average "cell" size = 190 microns, as opposed to dendrite arm spacing in ground-specimen # 1-4 equal to 25-35 microns). The geometry of this microstructure indicates low convection that would have otherwise disrupted the dendritic growth. The specimen lost a substantial fraction of its silver content during this long heating (0.57 wt% Ag in SL-2.4 and 0.85 wt% Ag in ground-specimen # 1-4). Extensive grain growth took place because of slow cooling of the solid and high purity (grain size = 1010 microns in SL-2.4 and only 305 microns in ground-specimen # 1-4). Some coarse silver particles that formed monotectically were detected between dendrite cells. Microhardness in SL-2.4 was on the average = 115 VHN, as compared with that in ground-specimen # 1-4, equal to 138 VHN. This property should be correlated with the total silver content of the specimen. The extreme smoothness of the SL-2.4 specimen may be attributed to the very small number of grain boundaries that outcrop on the surface, and to the absence of surface dendrites or interdendritic shrinkage.

Conclusions

The anticipated undercooling prior to nucleation of the melt was not observed in these specimens, because the melt was in contact with unmelted material in four cases (specimens SL-1.2, SL-1.12, SL-1.13 and SL-2.8) and with the retaining sting in the fifth case (specimen SL-2.4).

The specimens offered no positive microstructural evidence of any appreciable reduction in liquid convection. Some indications are given by specimen SL-2.4.

Substantial loss of silver by evaporation took place. Evaporation of silver within internal gas cavities in the melt was followed by surface condensation after completion of solidification and cooling, leading to formation of a silver-rich lining of these cavities.

The monotectic solidification sequence appears quite analogous to that observed on earth in vacuum.

References

1. D. Larson, "Phase-C Report. Evaluation of Skylab Specimens," Grumman Aerospace Corporation.

2. P. Johnson, "Phase-C Report. Evaluation of Skylab Specimens," A. D. Little, Inc.

3. T. Z. Kattamis, "Phase-C Report. Evaluation of Skylab Specimens," University of Connecticut.

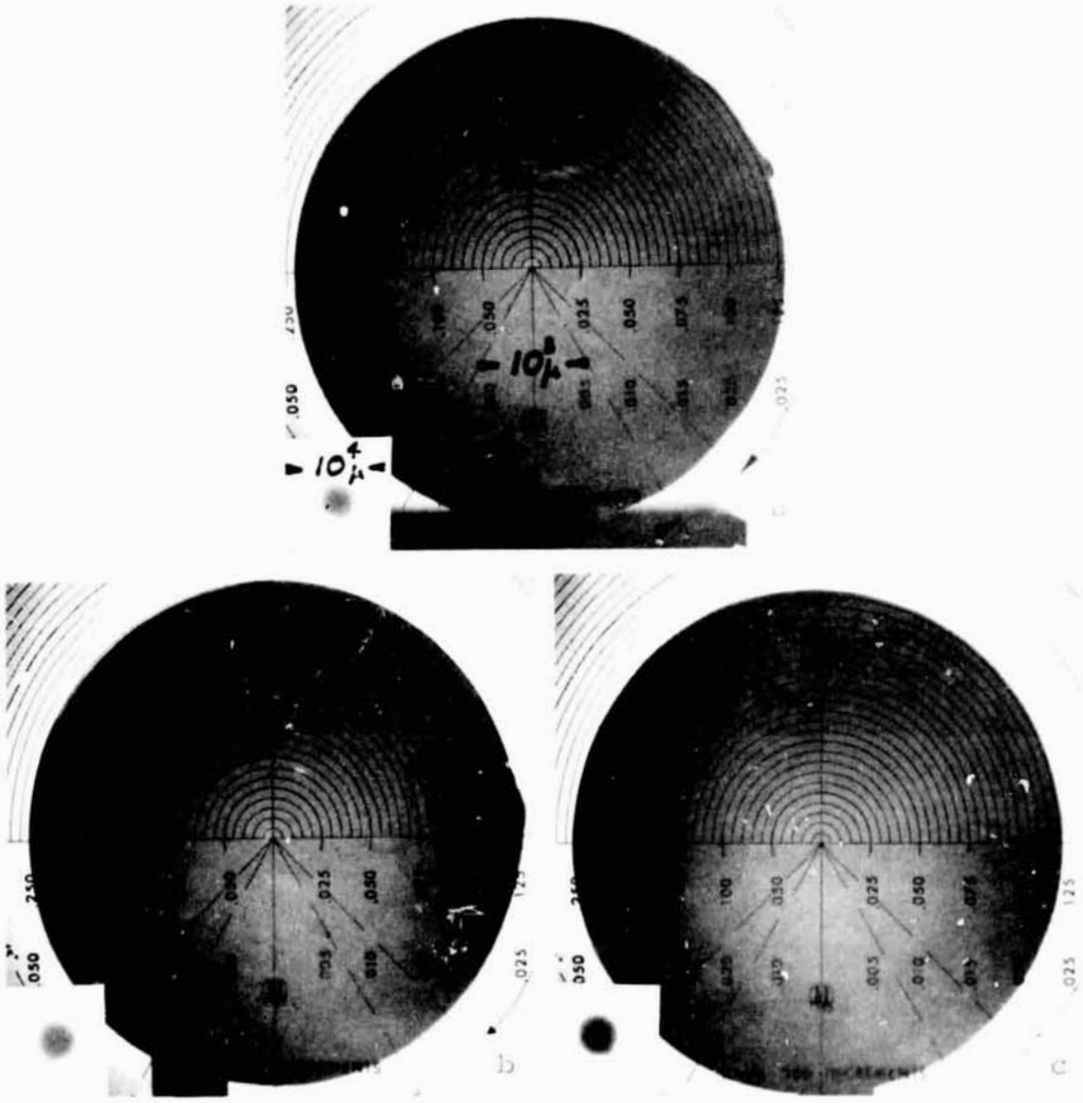

Figure 1. Shadowgraphs (10X) and X-ray macroradiographs (1X) of specimen SL-2.4. (a) Top views, (b) and (c) side views.

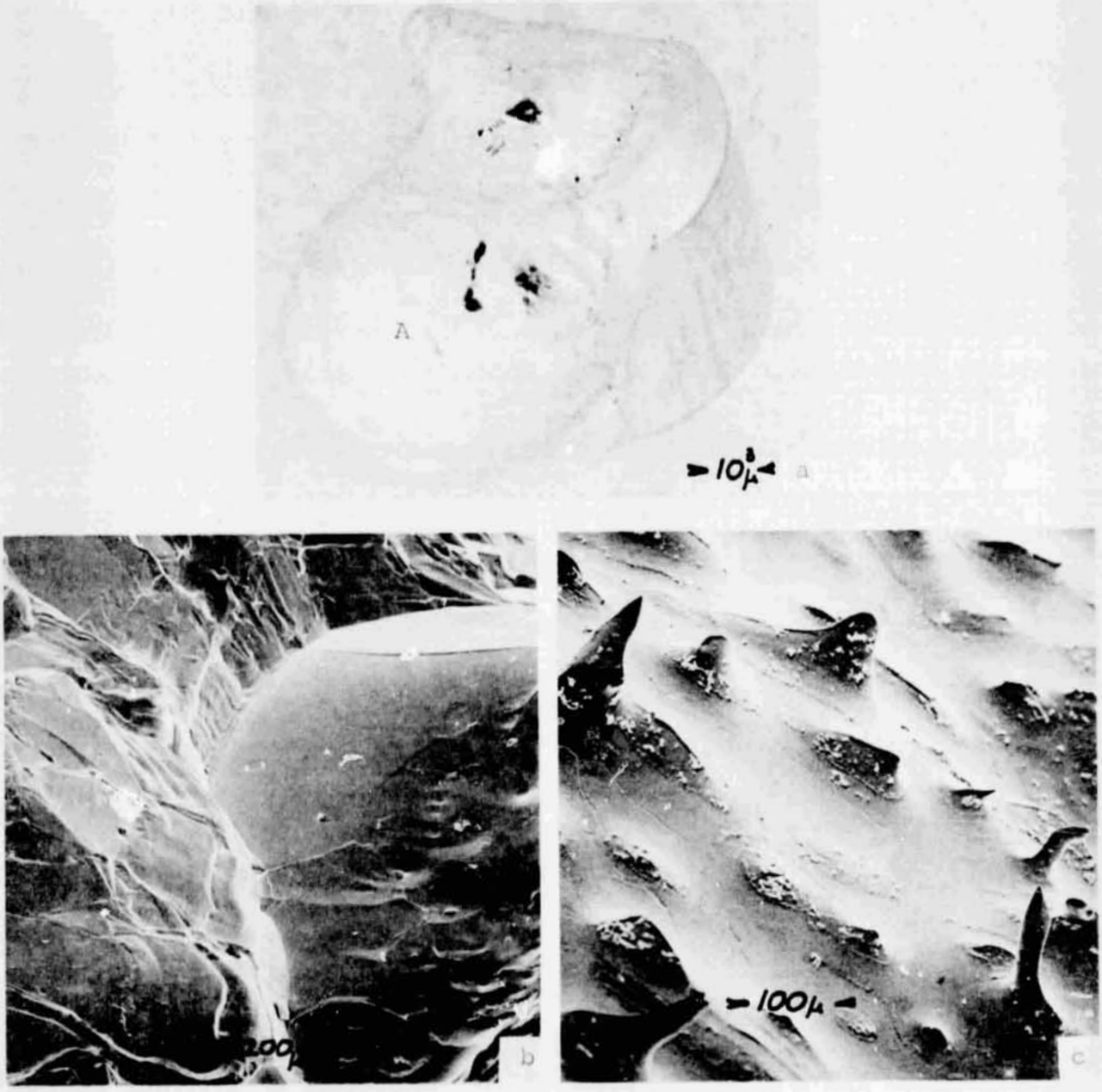

Figure 2. Scanning electron micrographs of specimen SL-1.13. (a) 10X, (b) 50X and (c) 150X. Courtesy of Grumman Aerospace Corporation.

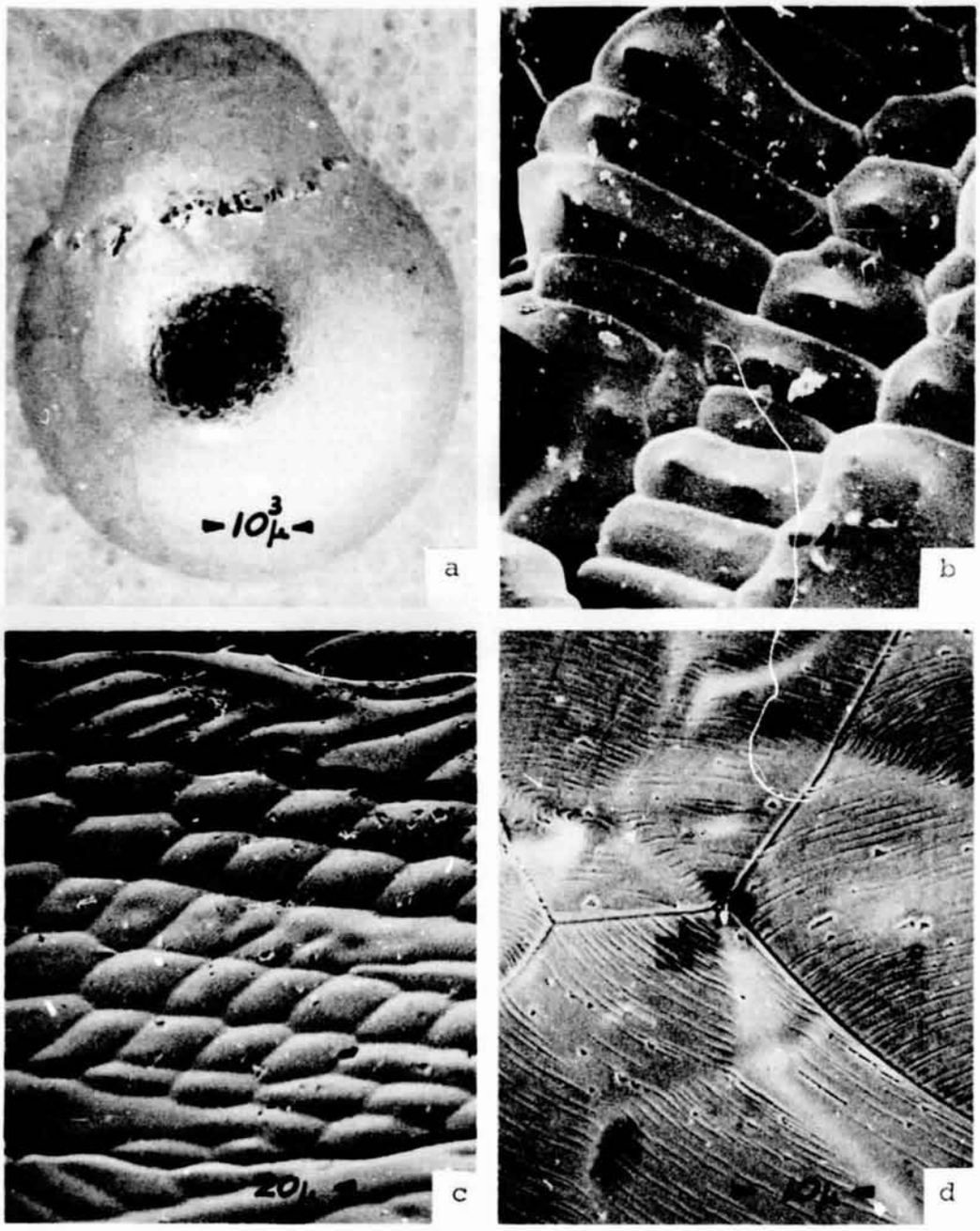

Figure 3. Scanning electron micrographs of specimen SL-1.2. (a) 10X, (b) dendritic morphology within a cavity, 250X, (c) cellular solidification pattern within the web of the specimen, 750X, and (d) inner surface patterns in upper cavity, 1500X. Courtesy of Grumman Aerospace Corporation.

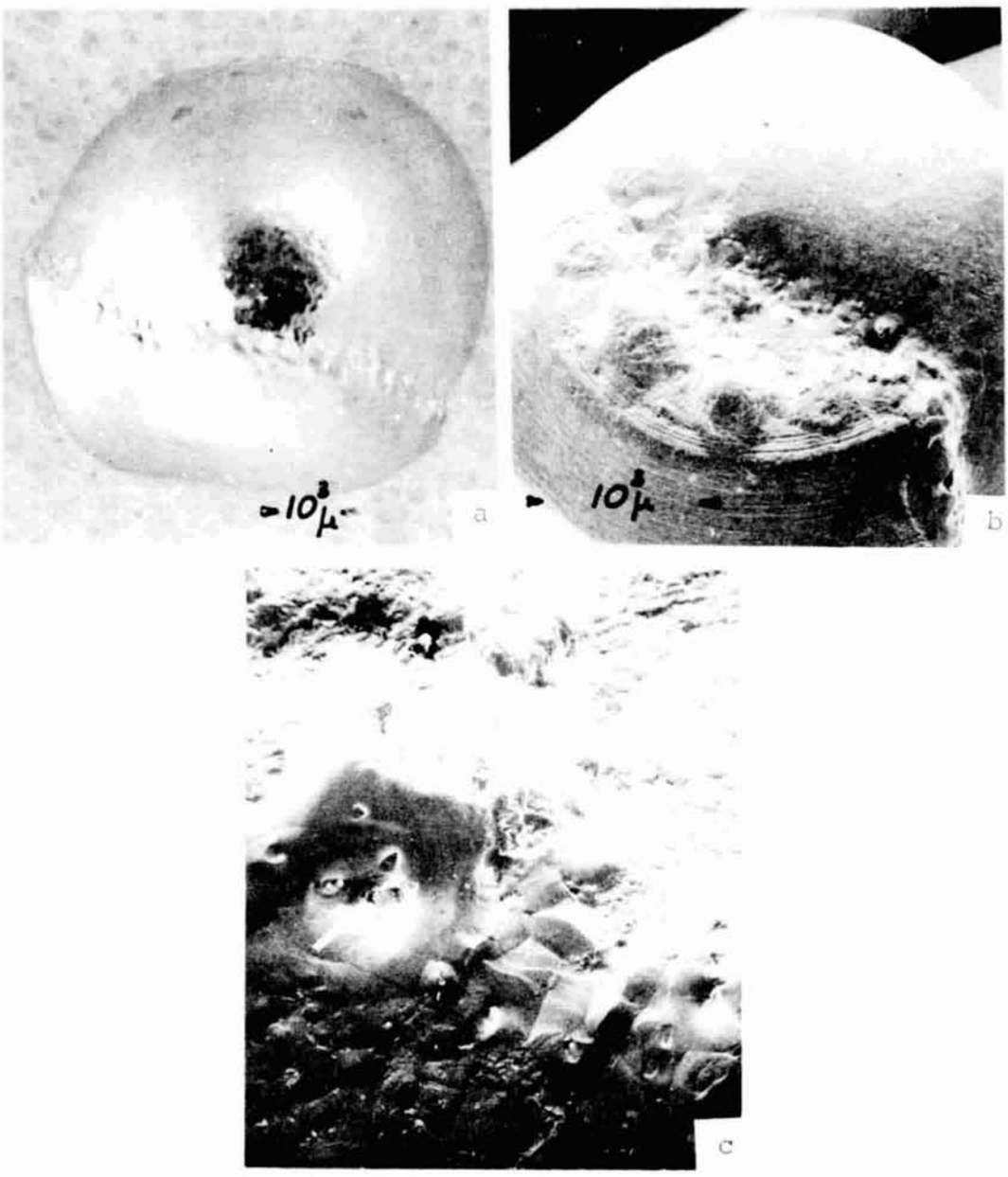

Figure 4. Scanning electron micrographs of specimen SL-2.8. (a) 10X, (b) 25X and (c) 100X.

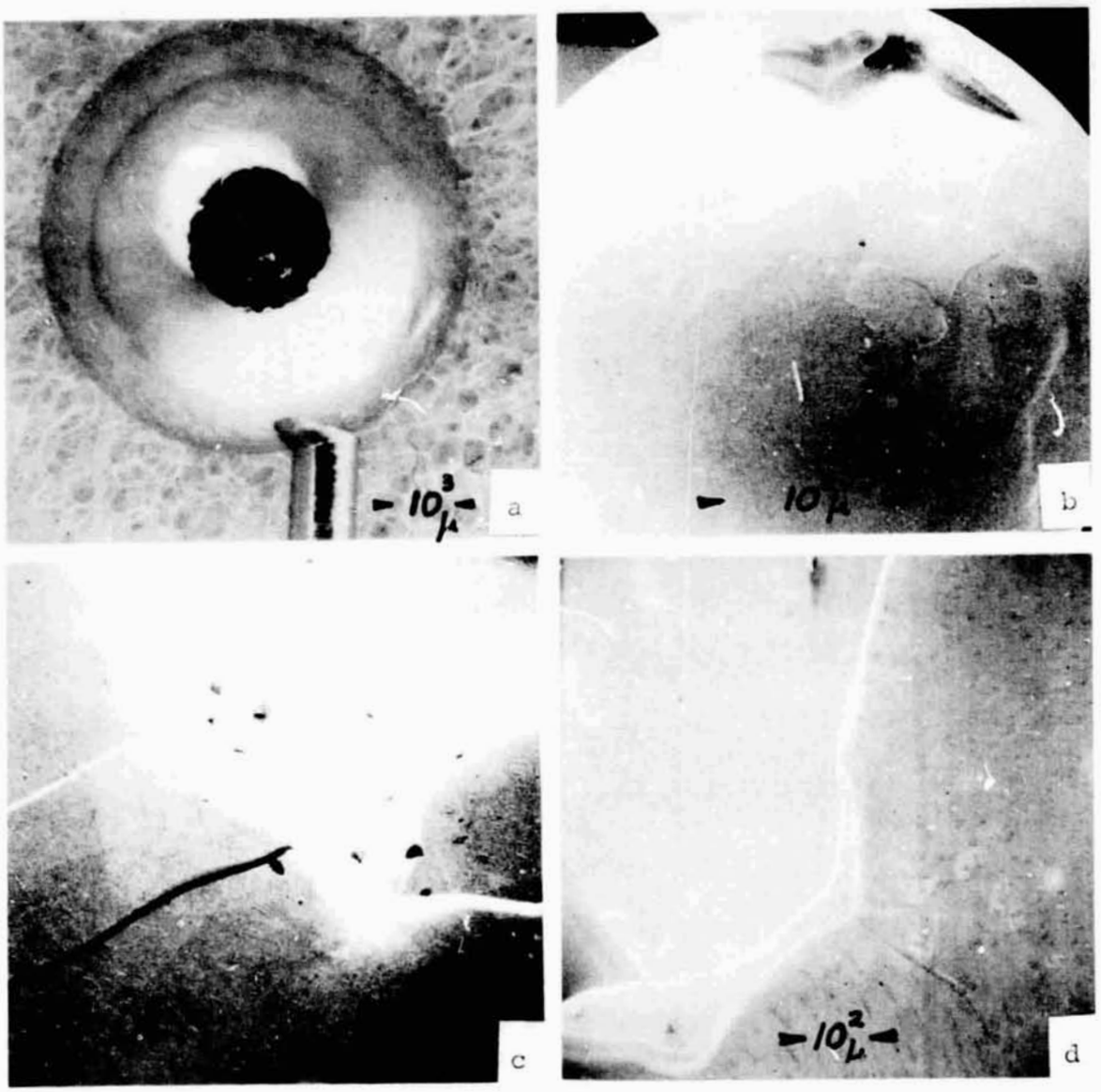

Figure 5. Scanning electron micrographs of specimen SL-2.4. (a) 10X, (b) 25X, (c) and (d) 100X.

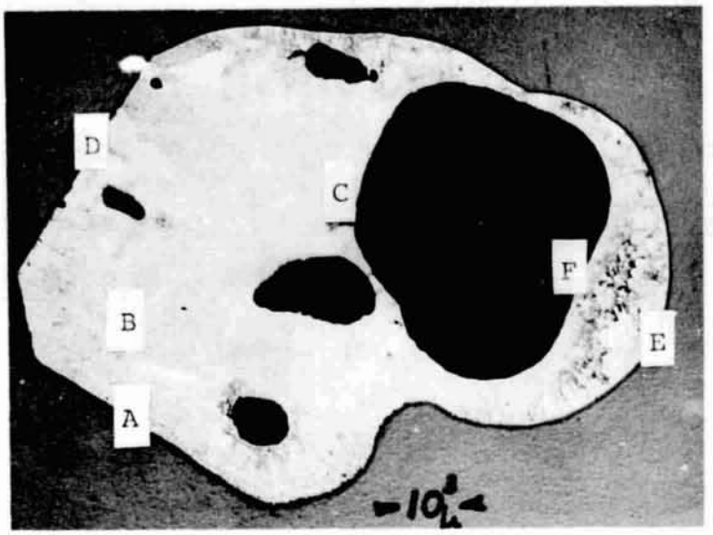

SPECIMEN SL-1.12

SPECIMEN SL-2.4

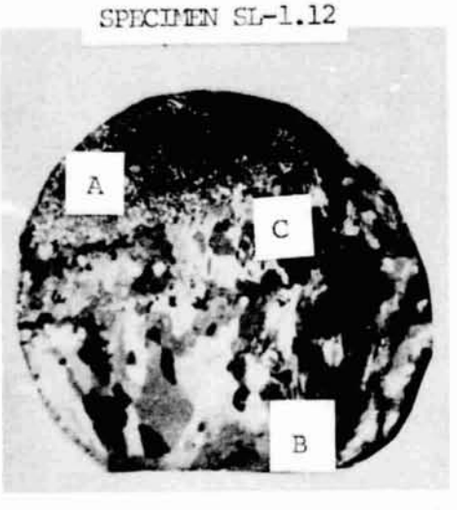

SPECIMEN SL-2.8

Figure 6. Photomicrographs illustrating the microstructure of specimen SL-1.12 (Courtesy of A. D. Little, Inc.) and of specimens SL-2.4 and SL-2.8, 10X.

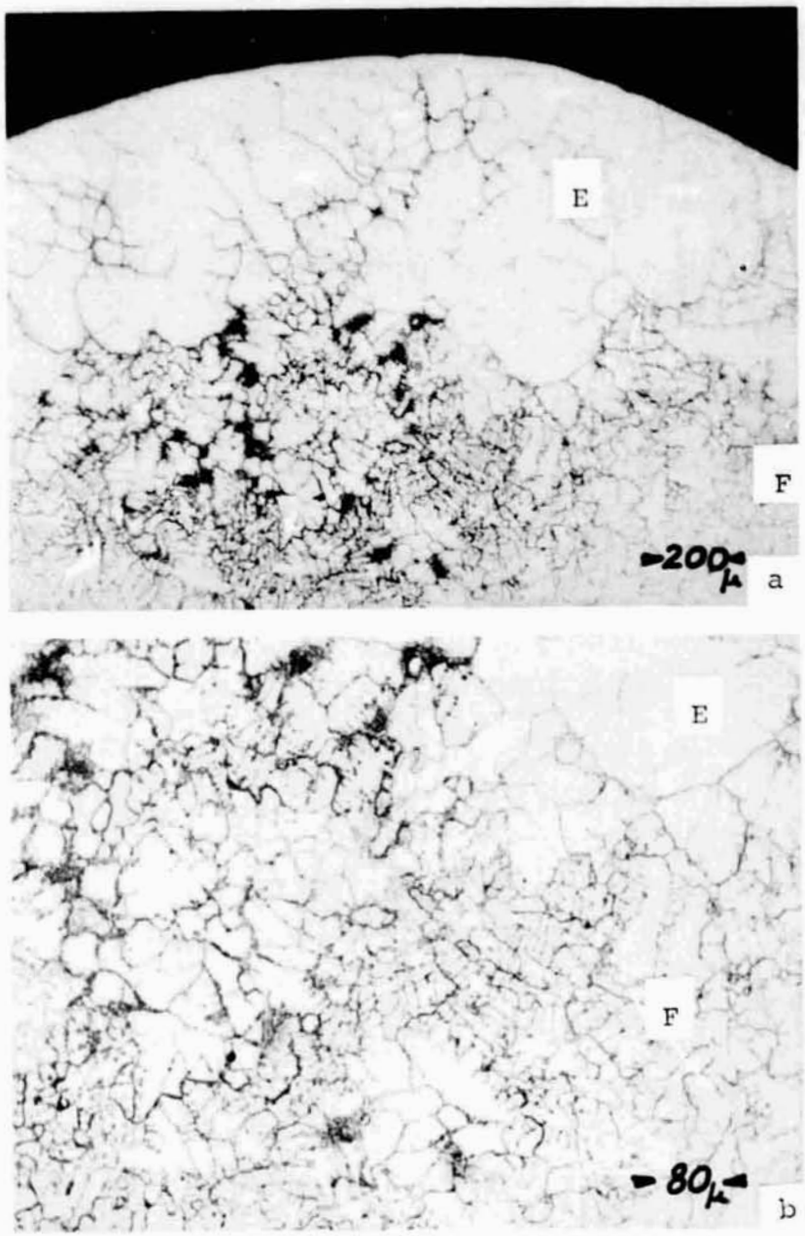

Figure 7. Photomicrographs of specimen SL-1.12. (a) 50X, (b) 125X. Courtesy of A. D. Little, Inc.

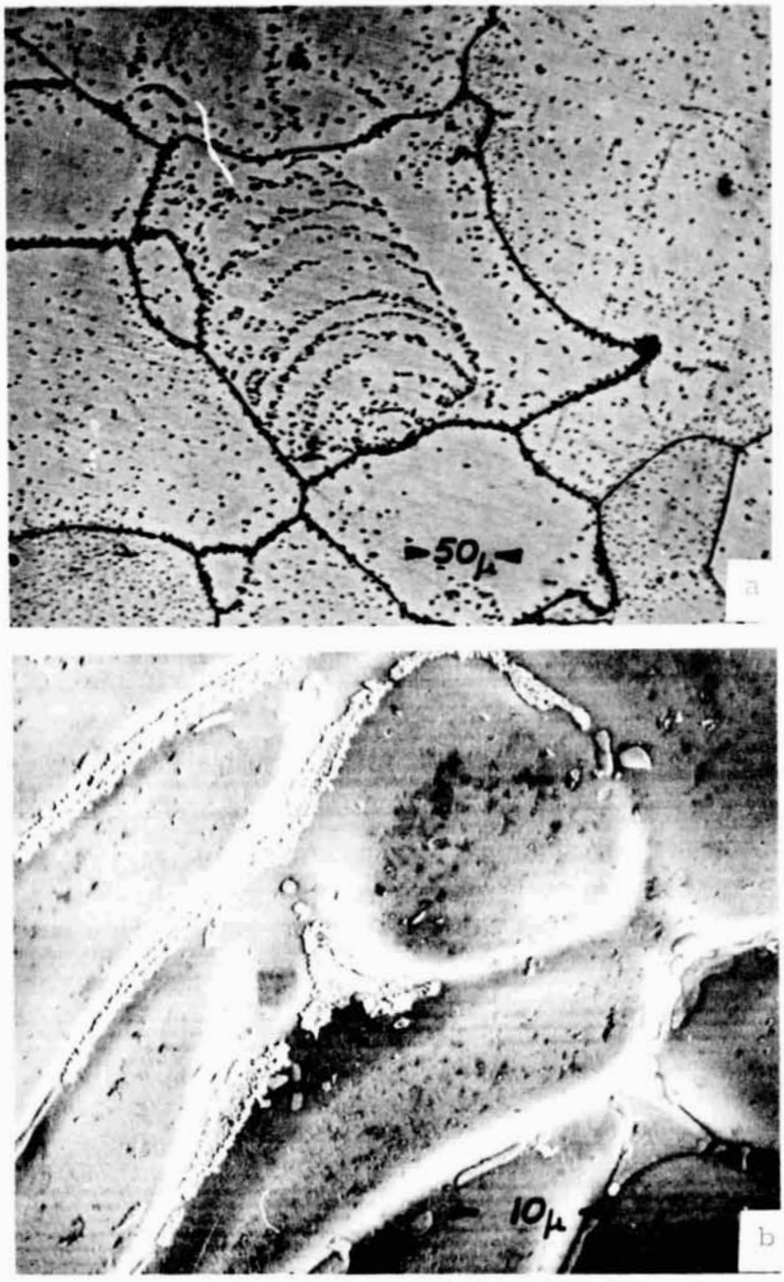

Figure 8. (a) Photomicrograph of specimen SL-1.13, 200X.
(b) Scanning electron micrograph of specimen SL-1.13, 1500X.

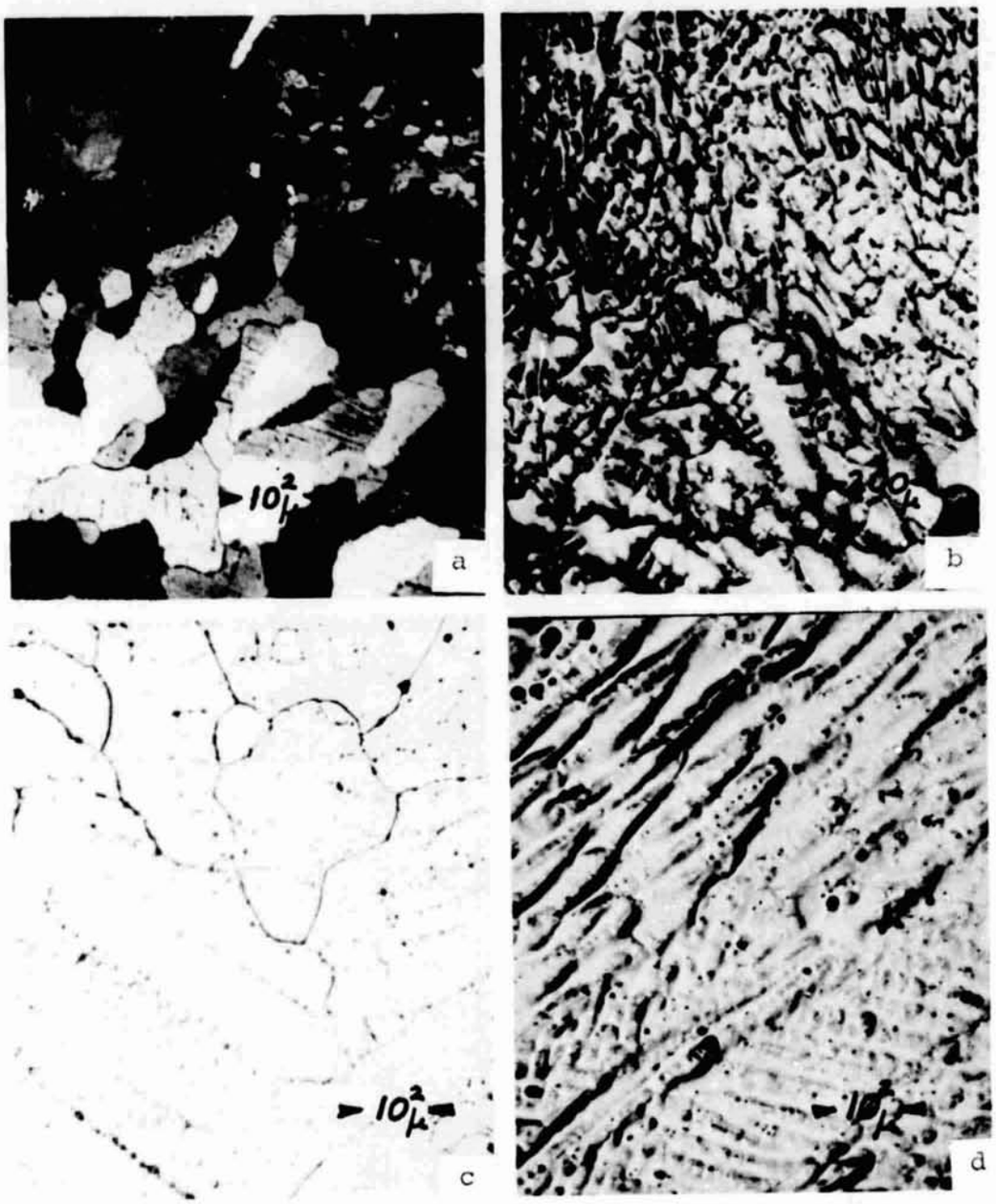

Figure 9. Photomicrographs of specimen SL-2.8. (a) Polarized light, 100X, (b) 50X, (c) and (d) 100X.

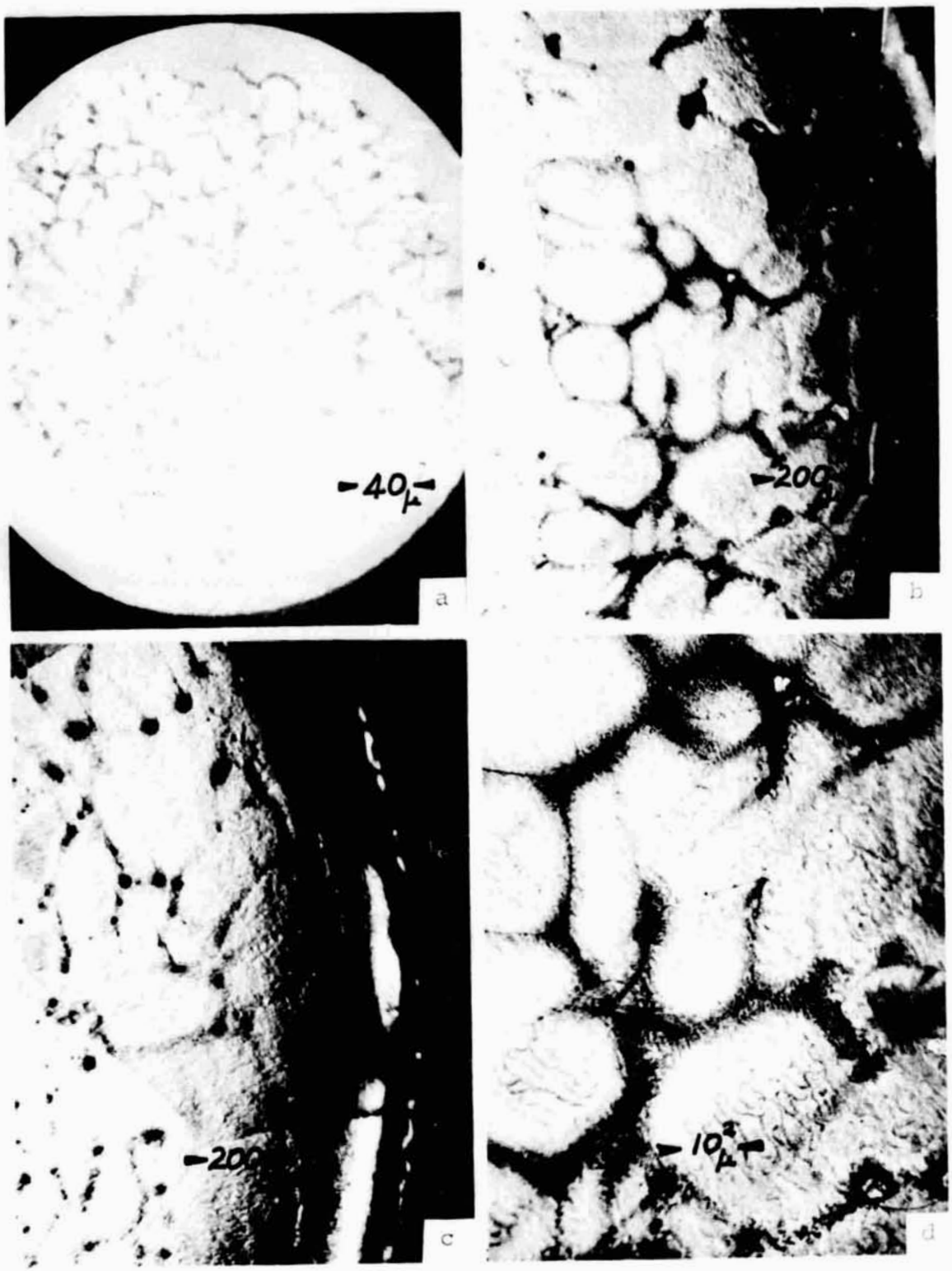

Figure 10. Photomicrographs of specimen SL-2.4 etched with Rosenhain's reagent. (a) 25X, (b) and (c) 50X and (d) 100X.

☆U.S. GOVERNMENT PRINTING OFFICE 1974 — 640 446 / 108 REGION NO. 4